JACS
JOURNAL OF THE AMERICAN CHEMICAL SOCIETY
Communication
pubs.acs.org/JACS

Stabilized Gold Nanoparticles on Ceria Nanorods by Strong Interfacial Anchoring

Na Ta,[†] Jingyue (Jimmy) Liu,*[,†,‡] Santhosh Chenna,[§] Peter A. Crozier,[§] Yong Li,[†] Aling Chen,[†] and Wenjie Shen*[,†]

[†]State Key Laboratory of Catalysis, Dalian Institute of Chemical Physics, Chinese Academy of Sciences, Dalian 116023, China
[‡]Department of Physics and [§]School for Engineering of Matter, Transport and Energy, Arizona State University, Tempe, Arizona 85287, United States

Supporting Information

ABSTRACT: Au/CeO_2 catalysts are highly active for low-temperature CO oxidation and water–gas shift reaction, but they deactivate rapidly because of sintering of gold nanoparticles, linked to the collapse or restructuring of the gold–ceria interfacial perimeters. To date, a detailed atomic-level insight into the restructuring of the active gold–ceria interfaces is still lacking. Here, we report that gold particles of 2–4 nm size, strongly anchored onto rod-shaped CeO_2, are not only highly active but also distinctively stable under realistic reaction conditions. Environmental transmission electron microscopy analyses identified that the gold nanoparticles, in response to alternating oxidizing and reducing atmospheres, changed their shapes but did not sinter at temperatures up to 573 K. This finding offers a new strategy to stabilize gold nanoparticles on ceria by engineering the gold–ceria interfacial structure, which could be extended to other oxide-supported metal nanocatalysts.

Since the discovery that nanosized gold particles, dispersed on metal oxides, are highly active for low-temperature CO oxidation,[1] extensive and intensive studies have been ongoing to understand the chemical nature of the active sites associated with the frequently observed high activities for an increasing number of reactions.[2] It is now generally acknowledged that the gold–oxide interfacial perimeter acts as the active site; the gold particles have to be smaller than 5 nm in order to obtain high activity, while the oxide support, especially reducible oxides, alters the catalytic property significanly.[2b,c,3] In this context, Au/CeO_2 catalysts have attracted particular attention because of their exceptionally high activities for low-temperature CO oxidation[4] and water–gas shift (WGS) reaction.[3b,5] The key function of ceria is to disperse and stabilize gold nanoparticles through its surface oxygen vacancies that strongly depend on the size and shape of ceria crystallites. For example, CeO_2 of 3–4 nm size with a large number of surface oxygen vacancies increased the CO oxidation rate of gold nanoparticles by 2 orders of magnitude.[4a] The use of CeO_2 nanorods that are rich in surface oxygen vacancies has greatly enhanced the activities of gold particles for low-temperature CO oxidation[4b,c] and WGS reaction.[5c] These highly active Au/CeO_2 catalysts, however, deactivated rapidly under realistic reaction conditions, primarily due to sintering of gold nanoparticles. Such a deactivation behavior is associated with the collapse or restructuring of the active gold–ceria interfaces, induced by the effects of temperature and reactive gases. Changes in the shape and size of gold nanoparticles in Au/CeO_2 catalysts have been examined both at elevated temperatures in a vacuum[6] and under reactive gases at ambient temperature.[7] However, changes in the active gold–ceria interface at practical temperatures and under reactive atmospheres were not well considered. Herein, we use atomic resolution environmental transmission electron microscopy (ETEM) to directly observe the structural changes of the Au/CeO_2 catalyst under conditions close to those of the reaction. Gold particles of 2–4 nm size, in response to alternating oxidizing and reducing atmospheres, changed their shapes but did not sinter at temperatures up to 573 K due to the strong interfacial bonding on CeO_2. The visual evidence was correlated with the prominent stabilities of the Au/CeO_2 catalysts in low-temperature CO oxidation and WGS reaction and raised the possibility of stabilizing gold nanoparticles by engineering the gold–oxide interfacial anchoring pattern.

We recently reported that rod-shaped ceria had a much higher activity in CO oxidation than conventional spherical ceria, mainly because of the facile generation of more surface oxygen vacancies.[8] In this work, the CeO_2 nanorods were further calcined at 973 K in air to ensure their stable size and shape during the subsequent loading of gold particles and the reaction tests. Analyses of TEM images showed that the high-temperature-treated ceria nanorods were largely enclosed by {111} planes; the average width of the nanorods was ~8 nm, and their lengths ranged from 50 to 200 nm, with a surface area of 75 m^2/g (Figure S1 in the Supporting Information (SI)). Gold particles were then dispersed onto the ceria nanorods by a deposition–precipitation method (details in the SI). The size of the gold particles depended strongly on the temperature of calcination. For the Au/CeO_2 catalyst calcined at 573 K, labeled as Au-573, individual Au atoms, subnanometer-sized Au clusters (<1 nm), and faceted Au particles (1–3 nm) were all present, as clearly shown in the aberration-corrected high-angle annular dark-field scanning transmission electron microscopy (HAADF-STEM) images (Figures 1a,b and S2a). When the same sample was calcined at 673 K, referred to as Au-673, however, faceted gold particles with a narrow size distribution of 2–4 nm were

Received: October 19, 2012
Published: December 11, 2012

   dx.doi.org/10.1021/ja310341j | J. Am. Chem. Soc. 2012, 134, 20585–20588

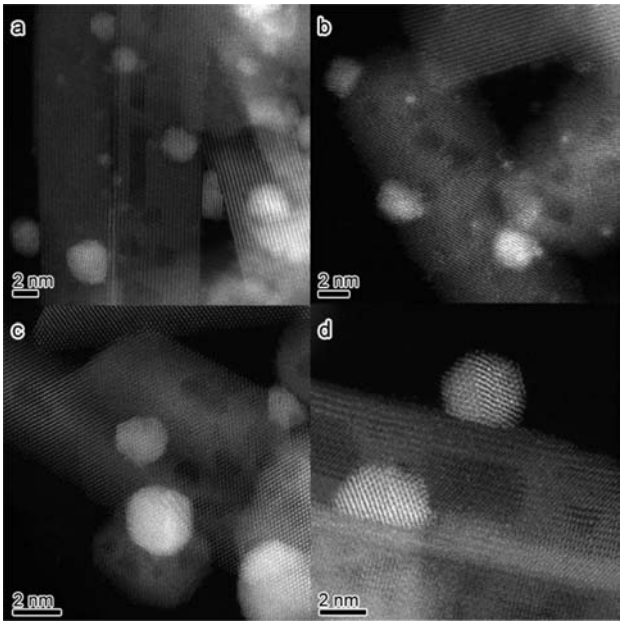

Figure 1. Aberration-corrected HAADF-STEM images of (a,b) subnanometer-sized Au clusters (<1 nm) and faceted Au particles (<3 nm) in the Au-573 catalyst and (c,d) faceted Au particles in the Au-673 catalyst with a narrow size distribution of 2−4 nm.

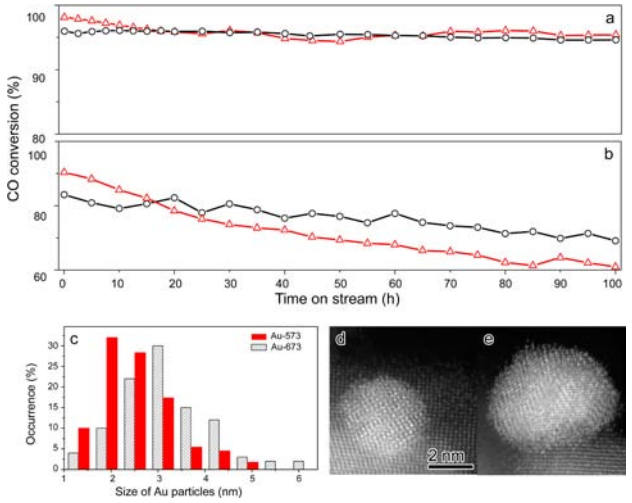

Figure 2. (a) CO oxidation at room temperature and (b) WGS reaction at 553 K on the Au-573 (red triangle) and Au-673 (black circle) catalysts. (c) Size distributions of Au particles in the used catalysts after the WGS reactions. (d,e) Aberration-corrected HAADF-STEM images of the used Au-573 (d) and Au-673 (e) catalysts, showing that the shape of the gold particles shifted to more rounded configurations.

observed; subnanometer-sized Au clusters were scarcely detectable (Figures 1c,d and S2b). These observations evidenced that higher temperature treatment enhanced the growth of gold clusters and particles, similar to the cases of gold species on ceria[6c] and iron oxides.[9] The evolution of Au particles or clusters is intimately associated with their bonding strength with surface oxygen vacancies on ceria, which has been verified experimentally[4a,c,5d] and predicted theoretically.[10] These surface oxygen vacancies on ceria have been proposed to be linear clusters that exclusively expose Ce^{3+} ions;[5d,11] they stabilize metal nanoparticles against sintering through strong chemical bonding.[12] Close inspection of the 2−4 nm gold particles in the Au-673 catalyst further identified that the Au{111}−CeO_2{111} interfaces had a preferential orientation relationship (Figure S2b). The gold columns were directly attached to the cerium columns, where the lattice fringes of both gold and ceria were clearly resolved; this type of anchoring was also observed for gold nanoparticles that grew epitaxially on two ceria nanorods. These results indicated that the gold nanoparticles interact strongly with the surfaces of the ceria nanorods.

The Au/CeO_2 catalysts were highly active and stable for CO oxidation at room temperature, with CO conversion of >95% for 100 h (Figure 2a). The slightly higher CO conversion during the initial 20 h on the Au-573 catalyst was primarily attributed to the presence of an appreciable amount of subnanometer-sized gold clusters that are intrinsically more active for CO oxidation.[9] When used for the WGS reaction at 553 K, the Au-573 catalyst showed a higher CO conversion at the initial 15 h, but the conversion of CO decreased remarkably thereafter and approached ∼60% after 100 h (Figure 2b). This reaction pattern demonstrated that the subnanometer-sized gold clusters were highly active, but they were not stable and easily sintered during the course of the WGS reaction. HAADF-STEM images of the used sample verified that the subnanometer-sized gold clusters in the fresh Au-573 catalyst had almost entirely disappeared and aggregated into faceted particles with a mean size of ∼2.8 nm (Figures 2c,d and S3a). On the other hand, the Au-673 catalyst, primarily consisting of gold particles with sizes in the 2−4 nm range, showed a slightly lower CO conversion during the initial stage of the WGS reaction but higher and more stable CO conversions after ∼15 h; the conversion of CO remained at ∼70% at the end of the operation (Figure 2b). This superior long-term performance of the Au-673 catalyst for the WGS reaction resulted from the presence of stable gold particles with sizes of 2−4 nm. The gold nanoparticles in the used catalyst after 100 h of the WGS reaction still had a mean size of ∼3.4 nm and were strongly anchored onto the CeO_2 surfaces. However, the shape of the gold particles distinctly shifted from the original truncated octahedral to more rounded configurations (Figures 2c,e and S3b). This shape variation of gold nanoparticles reflected the restructuring of the active gold−ceria interfaces under the reaction conditions.

The major challenge in developing practical Au/CeO_2 catalysts for the WGS reaction is the rapid deactivation. Although conclusive deactivation mechanisms are missing because of the complexities of the varied reaction temperatures and atmospheres, sintering of gold nanoparticles has been commonly observed.[5a,13] Lanthana-doped ceria alleviated the deactivation during the WGS reaction, but enlarged gold particles were clearly seen in the used catalyst.[13a] Gold nanoparticles on ceria−zirconia exhibited very high initial WGS activity, but they soon detached from the oxide support, reducing the gold−ceria interfacial area and consequently the loss of activity.[13b] Therefore, mitigation of the deactivation necessitates the enhancement of gold−ceria bonding strength. The salient stability achieved on the Au-673 catalyst indicates that the gold−ceria interfaces were more resistant toward deactivation under the WGS reaction conditions, probably involving the strong anchoring of gold nanoparticles of 2−4 nm size on CeO_2 nanorods.

The Au−CeO_2 interface perimeter has been generally viewed as the active site for both low-temperature CO oxidation and the WGS reaction.[2c,3b,5d,7b] The gold particle adsorbs CO, while the ceria support activates molecular oxygen or water through the participation of its lattice oxygen. Our isotopic ^{18}O kinetic experiments reaffirmed such a redox mechanism. On exposing

dx.doi.org/10.1021/ja310341j | J. Am. Chem. Soc. 2012, 134, 20585−20588

the Au-673 catalyst to CO, CO_2 was immediately produced, indicating that the CeO_2 nanorods supplied of reactive oxygen species to oxidize CO (Figure 3a). $^{18}O_2$ pulse restored the

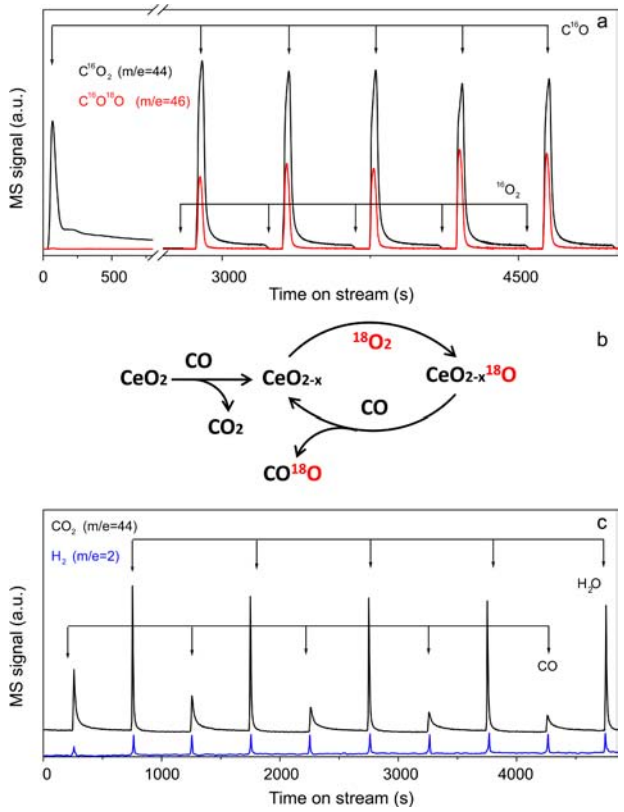

Figure 3. (a) Mass spectra during CO and $^{18}O_2$ sequential pulses over the Au-673 catalyst at 573 K. (b) Redox cycle of CeO_2 involving the participation of its lattice oxygen. (c) Mass spectra during CO and H_2O sequential pulses over the Au-673 catalyst at 573 K, demonstrating the redox cycle of CeO_2 in the WGS reaction.

stoichiometry of ceria and simultaneously activated molecular oxygen. During the subsequent alternating injections of CO and $^{18}O_2$ pulses, the production of $C^{16}O^{18}O$ molecules evidenced that the labeled oxygen atoms had incorporated into the ceria lattice during the redox cycle (Figure 3b). As the reaction pathways of CO oxidation and WGS reaction are similar, this isotopic experiment might be applicable to the WGS reaction as well, in which CO is adsorbed on gold nanoparticles and water is activated on the ceria surface (Figure 3c).

To understand the restructuring of the gold−ceria interfaces under the reaction conditions, we used ETEM to directly observe the structural changes of the Au-673 catalyst under oxidizing and reducing (reactive) atmospheres at 573 K. Under an oxidizing gas mixture (10 vol% O_2/N_2), the gold−ceria interfaces retained their original configuration without appreciable variation in shape or size; the gold particles rotated and twisted locally but did not disengage from the ceria surface to form agglomerates. Figure 4a shows a truncated octahedral Au particle of ∼3 nm size directly connected with ceria without any transition layers; the interfacial regions were rather stable, as evidenced by the clear distinction of the Au{111} and CeO_2{111} lattice fringes. With prolonged observation time, there were no obvious changes in the shape and size of the gold particle (Figure S4a). When the same Au particle was exposed to a reducing but reactive environment (42 vol% CO/6 vol% O_2/N_2), however, the gold−

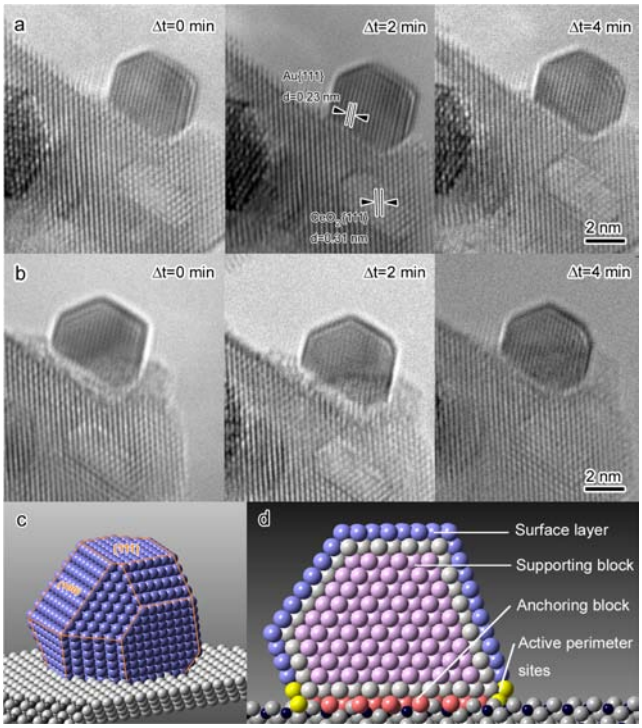

Figure 4. ETEM images of the Au-673 catalyst under oxidizing and reducing atmospheres at 573 K. (a,b) A truncated octahedral Au particle of ∼3 nm size under a 10 vol% O_2/N_2 environment (a) and a 42 vol% CO/6 vol% O_2/N_2 atmosphere (b). (c) Schematic depicting a typical gold nanoparticle enclosed by {111} and {100} planes. (d) Atomic scheme of a gold nanoparticle anchoring onto a CeO_2 nanorod, illustrating the functions of different domains.

ceria interfaces reconstructed with the appearance of disordered CeO_2 layers adjacent to the gold particle; the disordered ceria layers increased in thickness over time, and the gold particle was heavily reshaped (Figure S4b). This structural evolution was more clearly shown for another gold particle of ∼3 nm size (Figure S5). The chemical nature of the newly formed ceria layers was identified as $CeO_{1.714}$, and these partially reduced ceria species bonded the gold particle more tightly and probably changed the electronic state of gold, especially the gold atoms at the perimeter of the gold−ceria interface.[14]

The visual evidence provided deep insights into the restructuring of the gold−ceria interfaces: the modification in the gold−ceria interface is largely induced by the redox state of the underlying ceria support. As shown in Figure 2a, under oxidizing conditions typical of CO oxidation in rich oxygen, the gold−ceria interface worked dynamically but without obvious variations in size or shape of gold particles and thus kept rather stable performance. Under reducing and reactive atmospheres, similar to the case of WGS reaction, a CO molecule adsorbed on the gold particle and reacted with oxygen species on ceria at the interfacial region to form CO_2, generating oxygen-vacancy-dominated ceria surfaces. A water molecule replenished the oxygen-depleted ceria partially and accomplished the redox cycle. During this dynamic process, the CeO_2 support reshaped the gold particle due to the tighter bonding on the produced oxygen vacancies but sufficiently prevented the migration and aggregation of gold particle, avoiding the commonly observed sintering. The bonding strength at the buried Au−CeO_2 interfaces, between the surface oxygen vacancies on the ceria nanorods and the gold particles, is so strong that the gold

dx.doi.org/10.1021/ja310341j | J. Am. Chem. Soc. 2012, 134, 20585−20588

particles could only rotate/vibrate locally but could not migrate to form aggregates. Such a strong interfacial bonding primarily benefits from the collective properties of the surface oxygen vacancies on the ceria nanorods and their intimate contact with the Au nanoparticles. For subnanometer-sized Au clusters or Au particles with sizes <2 nm, however, the interfacial regions, during the CO oxidation and WGS reactions, may be completely modified by the redox cycles of the ceria support, significantly weakening the anchoring of Au clusters or tiny particles to the ceria surfaces; the consequence of these dynamic interactions is the sintering of Au species.

On the basis of these findings, we propose an anchoring mechanism for the stable Au-673 catalyst: Au particles with sizes of 2−4 nm are strongly anchored by the buried interfaces through intimate contact with the surface oxygen vacancies on ceria. By analyzing the shapes of many gold nanoparticles and their interfacial structures with ceria nanorods (Figures 1 and S2), we propose that the Au-673 catalyst consists of mainly truncated octahedral gold nanoparticles enclosed by the {111} and {100} facets and anchored onto the {111} facets of the ceria nanorods (Figure 4c). The faceted Au nanoparticle is constructed of four different domains; each has its unique function (Figure 4d). The internal gold atoms within the Au particle can be simply regarded as supporting blocks; they do not directly contribute to the catalytic performance, but they can restructure to facilitate the reshaping of the entire particle. The surface or subsurface layers of Au atoms are responsible for the adsorption of CO molecules.[7] The Au atoms at the gold−ceria perimeters are the active sites for the recombination of adsorbed CO molecules and active oxygen species on ceria to form CO_2 molecules. The interfacial Au atoms away from the particle perimeter (buried interfacial atoms) strongly anchor onto the underlying surface oxygen vacancies on the ceria nanorods. Since this buried interfacial region is not perturbed during the catalytic reactions, such a strong interaction stabilizes the Au nanoparticles. This anchoring mechanism can explain the outstanding stability of the Au-673 catalyst with Au particles in the size range of 2−4 nm. The ceria support provided a large number of oxygen vacancies on its surfaces; the strong bonding of Au nanoparticles with such oxygen vacancies facilitates their stabilization. The redox cycle of ceria during the catalytic reactions reshaped the gold particle but did not interrupt the strong bonding of the buried interfaces between the gold atoms and the ceria surface. As a consequence, the shape change of the Au particle may slightly modify the interfacial gold−ceria bonding but may not weaken the bonding to the degree that the Au particles disengage from their original anchoring sites. This newly discovered anchoring mechanism, achieved by engineering the shape of ceria nanocrystals and their unique interactions with faceted gold nanoparticles, is general and could be extended to develop other types of oxide-supported metal nanoparticles with better stability.

■ ASSOCIATED CONTENT

Supporting Information

Materials and methods; further experimental data, including TEM images of the CeO_2 nanorods, HAADF-STEM images of the Au/CeO_2 catalysts before and after the WGS reactions, ETEM images and shape illustrations of the gold particles. This material is available free of charge via the Internet at http://pubs.acs.org.

■ AUTHOR INFORMATION

Corresponding Author

shen98@dicp.ac.cn; jingyue.liu@asu.edu

Notes

The authors declare no competing financial interest.

■ ACKNOWLEDGMENTS

This work was supported by the National Natural Science Foundation of China (20923001, 21025312, and 21103172). J.L. acknowledges the start-up fund of the College of Liberal Arts and Sciences of Arizona State University and the use of the TEM/STEM at the John M. Cowley Center for High Resolution Microscopy at Arizona State University.

■ REFERENCES

(1) (a) Haruta, M.; Kobayashi, T.; Sano, H.; Yamada, N. *Chem. Lett.* **1987**, *16*, 405. (b) Haruta, M.; Yamada, N.; Kobayashi, T.; Iijima, S. J. *Catal.* **1989**, *115*, 301. (c) Haruta, M. *Nature* **2005**, *437*, 1098.

(2) (a) Fu, Q.; Saltsburg, H.; Flytzani-Stephanopoulos, M. *Science* **2003**, *301*, 935. (b) Hutchings, G. J. *Gold Bull.* **2009**, *42*, 260. (c) Haruta, M. *Faraday Discuss.* **2011**, *152*, 11.

(3) (a) Chen, M. S.; Goodman, D. W. *Acc. Chem. Res.* **2006**, *39*, 739. (b) Rodriguez, J. A.; Ma, S.; Liu, P.; Hrbek, J.; Evans, J.; Pérez, M. *Science* **2007**, *318*, 1757. (c) Zhou, Z.; Kooi, S.; Flytzani-Stephanopoulos, M.; Saltsburg, H. *Adv. Funct. Mater.* **2008**, *18*, 2801. (d) Campbell, C. T.; Sharp, J. C.; Yao, Y. X.; Karp, E. M.; Silbaugh, T. L. *Faraday Discuss.* **2011**, *152*, 227. (e) Bond, G. C. *Faraday Discuss.* **2011**, *152*, 277.

(4) (a) Carrettin, S.; Concepcion, P.; Corma, A.; Nieto, J. M. L.; Puntes, V. F. *Angew. Chem., Int. Ed.* **2004**, *43*, 2538. (b) Huang, X. S.; Sun, H.; Wang, L. C.; Liu, Y. M.; Fan, K. N.; Cao, Y. *Appl. Catal., B* **2009**, *90*, 224. (c) Lee, Y.; He, G.; Akey, A. J.; Si, R.; Flytzani-Stepanopoulos, M.; Herman, I. P. *J. Am. Chem. Soc.* **2011**, *133*, 12952.

(5) (a) Kim, C. H.; Thompson, L. T. *J. Catal.* **2005**, *230*, 66. (b) Kim, C. H.; Thompson, L. T. *J. Catal.* **2006**, *244*, 248. (c) Si, R.; Flytzani-Stephanopoulos, M. *Angew. Chem., Int. Ed.* **2008**, *47*, 2884. (d) Vindigni, F.; Manzoli, M.; Damin, A.; Tabakova, T.; Zecchina, A. *Chem. Eur. J.* **2011**, *17*, 4356.

(6) (a) Majimel, J.; Lamirand-Majimel, M.; Moog, I.; Feral-Martin, C.; Tréguer-Delapierre, M. *J. Phys. Chem. C* **2009**, *113*, 9275. (b) Akita, T.; Tanaka, S.; Tanaka, K.; Kohyama, M. *Mater. Sci. Forum* **2010**, *654−656*, 2362. (c) Akita, T.; Tanaka, S.; Tanaka, K.; Haruta, M.; Kohyama, M. *J. Mater. Sci.* **2011**, *46*, 4384.

(7) (a) Uchiyama, T.; Yoshida, H.; Kuwauchi, Y.; Ichikawa, S.; Shimada, S.; Haruta, M.; Takeda, S. *Angew. Chem., Int. Ed.* **2011**, *50*, 10157. (b) Yoshida, H.; Kuwauchi, Y.; Ichikawa, S.; Jinschek, J. R.; Sun, K.; Tanaka, S.; Kohyama, M.; Shimada, S.; Haruta, M.; Takeda, S. *Science* **2012**, *335*, 317.

(8) Tana, Z. M.; Li, J.; Li, H.; Li, Y.; Shen, W. *Catal. Today* **2009**, *148*, 179.

(9) Herzing, A. A.; Kiely, C. J.; Carley, A. F.; Landon, P.; Hutchings, G. J. *Science* **2008**, *321*, 1331.

(10) (a) Zhang, C.; Michaelides, A.; Jenkins, S. J. *Phys. Chem. Chem. Phys.* **2011**, *13*, 22. (b) Chen, Y.; Wang, H.; Burch, R.; Hardacre, C.; Hu, P. *Faraday Discuss.* **2011**, *152*, 121.

(11) (a) Esch, F.; Fabris, S.; Zhou, L.; Montini, T.; Africh, C.; Fornasiero, P.; Comelli, G.; Rosei, R. *Science* **2005**, *309*, 752. (b) Liu, X.; Zhou, K.; Wang, L.; Wang, B.; Li, Y. *J. Am. Chem. Soc.* **2009**, *131*, 3140.

(12) Farmer, J. A.; Campbell, C. T. *Science* **2010**, *329*, 933.

(13) (a) Fu, Q.; Deng, W.; Saltsburg, H.; Flytzani-Stephanopoulos, M. *Appl. Catal., B* **2005**, *56*, 57. (b) Goguet, A.; Burch, R.; Chen, Y.; Hardacre, C.; Hu, P.; Joyner, R. W.; Meunier, F. C.; Mun, B. S.; Thompsett, D.; Tibiletti, D. *J. Phys. Chem. C* **2007**, *111*, 16927.

(14) (a) Miguel, L. H; José, M. C.; Susana, T.; José, A. P. O.; Juan, J. D.; Serafín, B.; Pascale, B. G.; Odile, S.; Kenta, Y.; Edward, D. B.; Pratibha, L. G.; José, J. C. *ACS Nano* **2012**, *6*, 6812. (b) Alessandro, L.; Leonarda, F. L.; Giuseppe, P.; Francesco, G.; Anna, M. V.; Antonino, M. *J. Phys. Chem. C* **2012**, *116*, 2960.